Self-assembly and properties of diblock copolymers by coarse-grain molecular dynamics

GOUNDLA SRINIVAS[1,3], DENNIS E. DISCHER[2,3] AND MICHAEL L. KLEIN[1,3]*

[1]Center for Molecular Modeling, Department of Chemistry, University of Pennsylvania, Philadelphia 19104-6323, USA
[2]Department of Chemical & Biomolecular Engineering, University of Pennsylvania, Philadelphia 19104-6315, USA
[3]Laboratory for Research on the Structure of Matter, University of Pennsylvania, Philadelphia 19104-6202, USA
*e-mail: klein@lrsm.upenn.edu

Published online: 8 August 2004; doi:10.1038/nmat1185

Block-copolymer amphiphiles have been observed to assemble into vesicles and other morphologies long known for lipids but with remarkably different properties. Coarse-grain molecular dynamics (CG-MD) is used herein to elaborate the structures and properties of diblock copolymer assemblies in water. By varying the hydrophilic/hydrophobic ratio of the copolymer in line with experiment, bilayer, cylindrical and spherical micelle morphologies spontaneously assemble. Varying the molecular weight (MW) with hydrophilic/hydrophobic ratio appropriate to a bilayer yields a hydrophobic core thickness that scales for large MW as a random coil polymer, in agreement with experiment. The extent of hydrophobic-segment overlap in the core increases nonlinearly with MW, indicative of chain entanglements and consistent with the dramatic decrease reported for lateral mobility in polymer vesicles. Calculated trends with MW as well as hydrophilic/hydrophobic ratio thus agree with experiment, demonstrating that CG-MD simulations provide a rational design tool for diblock copolymer assemblies.

Diblock copolymer amphiphiles are synthetically diverse and can span molecular weights (MW) orders of magnitude greater than natural surfactants. This allows for fundamentally new insights into properties and design principles of micelles and biomimetic membranes. Indeed, amphiphilic diblock copolymers with lipid-like hydrophilic/hydrophobic proportions are known to self-assemble into vesicles in water[1–3]. Moreover, many biological membrane processes such as protein insertion[4], fusion, DNA encapsulation[5], biocompatibility [6-8] and so on. have now been mimicked with synthetic polymer vesicles. Non-biological but useful functions such as vesicle degradability for controlled release have also been realized with hydrolysable and oxidizable copolymers[8]. By altering the diblock copolymer hydrophilic/hydrophobic structure, other morphologies such as worm-like or spherical micelles can also readily be made[9,10]. Although a polymer approach to vesicle and micelle formation certainly broadens the range of achievable properties, there is now an opportunity, challenge and need to provide predictive insight that is complementary to synthesis and characterization.

The use of block-copolymer membranes are motivated in part by the fact that lipid membranes are (by nature's design) limited in their stability, which undermines their utility in applications ranging from drug delivery to sensor development[11–17]. Whereas any great increase in hydrophobic fraction of a lipid will promote a transition from membranes to an inverted phase, block copolymers allow one to maintain critically important proportions of hydrophilicity to hydrophobicity[18,19]. Compared with biomembranes, a higher average copolymer MW is typical and yields hyperthick membranes. Polymer vesicles or 'polymersomes' have thus provided a novel opportunity to study membrane properties experimentally as a function of thickness. Mechanically, polymersome membranes sustain dilational strains up to 40–50% compared with ~5% or less for lipid membranes[1,2,17]. The aim here is to understand by molecular simulation the origin of such novel properties of polymersomes, as well as the microscopic basis for membrane formation versus other states of aggregation such as worms or micelles.

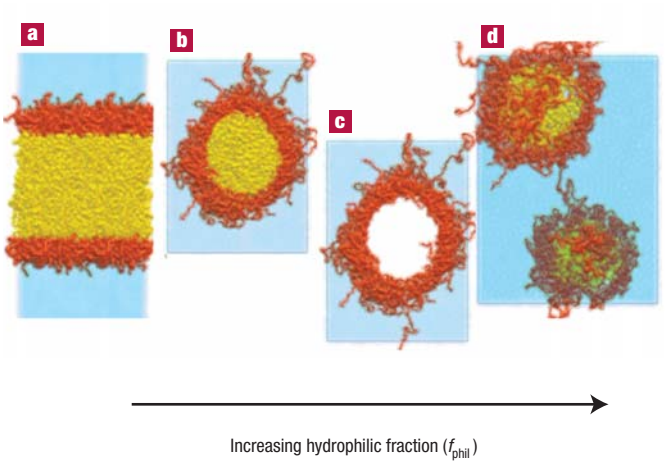

Figure 1 **Snap-shots taken from coarse-grain molecular dynamics simulations of diblock copolymers in water.** Distinct morphologies form spontaneously when the diblock copolymers have different hydrophilic fractions (f_{phil}). **a**, Bilayer assembly from 30.9% (w/w) hydrophilic moiety, $EO_{21}EE_{37}$. **b**, Cylindrical or worm-like micelle assembled from 51.1% hydrophilic moiety $EO_{50}EE_{37}$. **c**, Same as in **b** showing the hydrophilic EO corona but without the hydrophobic EE core; the cylindrical core extends through the periodic boundaries of the MD simulation cell. **d**, Spherical micelle formed from 65.6% hydrophilic moiety $EO_{92}EE_{37}$. Colour code: hydrophilic EO, red; hydrophobic EE, yellow; water, blue.

To date there have been no simulation studies of block-copolymer vesicles and micelles that come close to rationalizing the experimental findings on structure, dynamics and physical properties. Existing simulation studies have been carried out using model block copolymers with simplified potentials[20–25], motivating a more rigorous understanding of microscopic details. Molecular dynamics (MD) simulations on fully atomistic models are not possible because the timescale for spontaneous self-assembly is too long (microseconds) and because the system sizes are too large (many hundreds of thousands of atoms) to be routinely studied using currently available computers. On the other hand, overly simplistic polymer models will necessarily lack important details. Accordingly, in this study we rationally model both the block-copolymer segments and water using a stepwise coarse-grain (CG) approach that has demonstrated its utility in probing a variety of slow relaxing phenomena, such as surfactant[26] and membrane self-assembly and fusion[27–35]. The CG approach used herein allows one to probe longer length- and timescales of such systems while making direct connection to more rigorous atomistic schemes[28–37]. In this work, we report the salient results of our extensive CG-MD simulations of diblock copolymer self-assembly in water.

The important morphologies known to arise in diblock copolymer self-assembly have been observed to arise spontaneously in the present CG simulations (Fig. 1). As with experiments[10], the key is to increase the hydrophilic fraction of the copolymer. Bilayer and spherical micelle formation is observed at lower (f_{phil} < 45%) and higher (f_{phil} > 60%) hydrophilic weight fractions, respectively. Cylindrical (or worm-like) micelles are observed in a narrow range of intermediate hydrophilic weight fractions (45% < f_{phil} < 55%). The formation of a continuous worm-like micelle is evident from Fig. 1c.

A description of the CG parameterization is given in the Methods and in the Supplementary Information, so only the salient details are mentioned here. Figure 2 depicts the rational mapping of an all-atom polymer onto a CG model. Consecutive monomers in the CG polymer are linked by harmonic bond stretch and bend potentials that closely approximate atomistic bond lengths and angles, as shown in the insets of Fig. 2. The non-bonded interactions among the CG hydrophobic sites are modelled with a Lennard–Jones 9–6 potential, whereas tabulated potentials are used for the hydrophilic sites. Coarse-grain water is treated as a fluid of spherically symmetric particles (W), each representing a group of three water molecules. The relevant parameters for the bonded and non-bonded interaction potentials can be found in the Supplementary Information.

For the systematic study of bilayers as a function of MW, the CG-MD simulation system is constructed by replicating a basic unit of four copolymers plus sufficient W to fully hydrate the chains. All such systems were allowed to relax and equilibrate at 298.15 K for 5 ns of CG-MD. The stability of each bilayer is then monitored for a further 5 ns. Each run corresponds roughly to a microsecond of all-atom simulation. Because the surface tension is sensitive to the area per polymer[38,39] we used the N_APT ensemble[40,41], in which box lengths in the membrane plane (x, y directions) are held fixed. As a result, the normal pressure (z direction) fluctuates around a mean value, while keeping the area per polymer unchanged.

Goetz and Lipowsky[27,42] systematically studied bilayer states with small negative or positive tensions and thus have been able to interpolate towards tensionless states. By following their method we have determined the 'tensionless' states. To this end, in each case the initial simulation system having area per polymer (A = 113.1 Å^2) is both expanded (tension increases) and compressed (tension decreases) in the xy plane in order to generate a series of systems with different A. The in-plane tension in each system is determined according to[27,42],

$$\tau = \int_{-L_z/2}^{L_z/2} \mathrm{d}z\,[\tau_T(z) - \tau_N(z)] \qquad (1)$$

where the tangential and normal components of stress tensor are denoted by τ_T and τ_N, respectively. L_z is the box length along the z direction. Alternately, we have determined tension also by using the formula[43], $\tau = \langle (L_z/2)\,[(P_{zz} - (P_{xx} + P_{yy})/2)]\rangle$, where P_{ij} is the ij component of the pressure tensor. A simulation cell with zero net tension is determined and the properties obtained in that state are compared with experimental observations. All the relevant calculational details are mentioned in the Supplementary Information.

Discher and co-workers[1] observed that the hydrophobic thickness (d) of polymersome membranes has a power-law dependence $d = \Phi(MW_{phob})^{\varsigma}$, where MW_{phob} is the molecular weight of the hydrophobic moiety, Φ is a constant and $\varsigma \approx 1/2$. This scaling corresponds to ideal random-coil behaviour in the core. Fully stretched chains would have given ς = 1, whereas the long-established theory of strong segregation predicts ς = 2/3. The latter scaling is readily arrived at by minimizing (with respect to d) a free energy that contains a simple chain-elasticity term and an interfacial energy per chain ($\sim\gamma A$). Whereas the experimental studies that yield a scaling of $\varsigma \approx 1/2$ involved vesicle membranes of hydrophobic thickness $d \geq 8$ nm and copolymers of MW ≥ 3 kDa, scaling in simulation here for lower MW chains was also examined. Six different systems were studied using CG-MD, with MW ranging from 1 kDa to 7.28 kDa and with a nearly constant hydrophilic/hydrophobic ratio.

Density profiles of hydrophobic segments for all the systems (at τ = 0) are shown in Fig. 3a. As of yet, no such experimental measurements of the profiles have been made. However, a logarithmic relationship between MW_{phob} and thickness is shown in Fig. 3b, which compares the simulations directly to experiment. The full line is a linear fit through both simulation and experiment results. The slope of the scaling curve is obtained by fitting to the experimental results and simulations systems with d < 7 nm. Information on scaling can also be obtained by fitting with various cut-off values of d. The higher MW

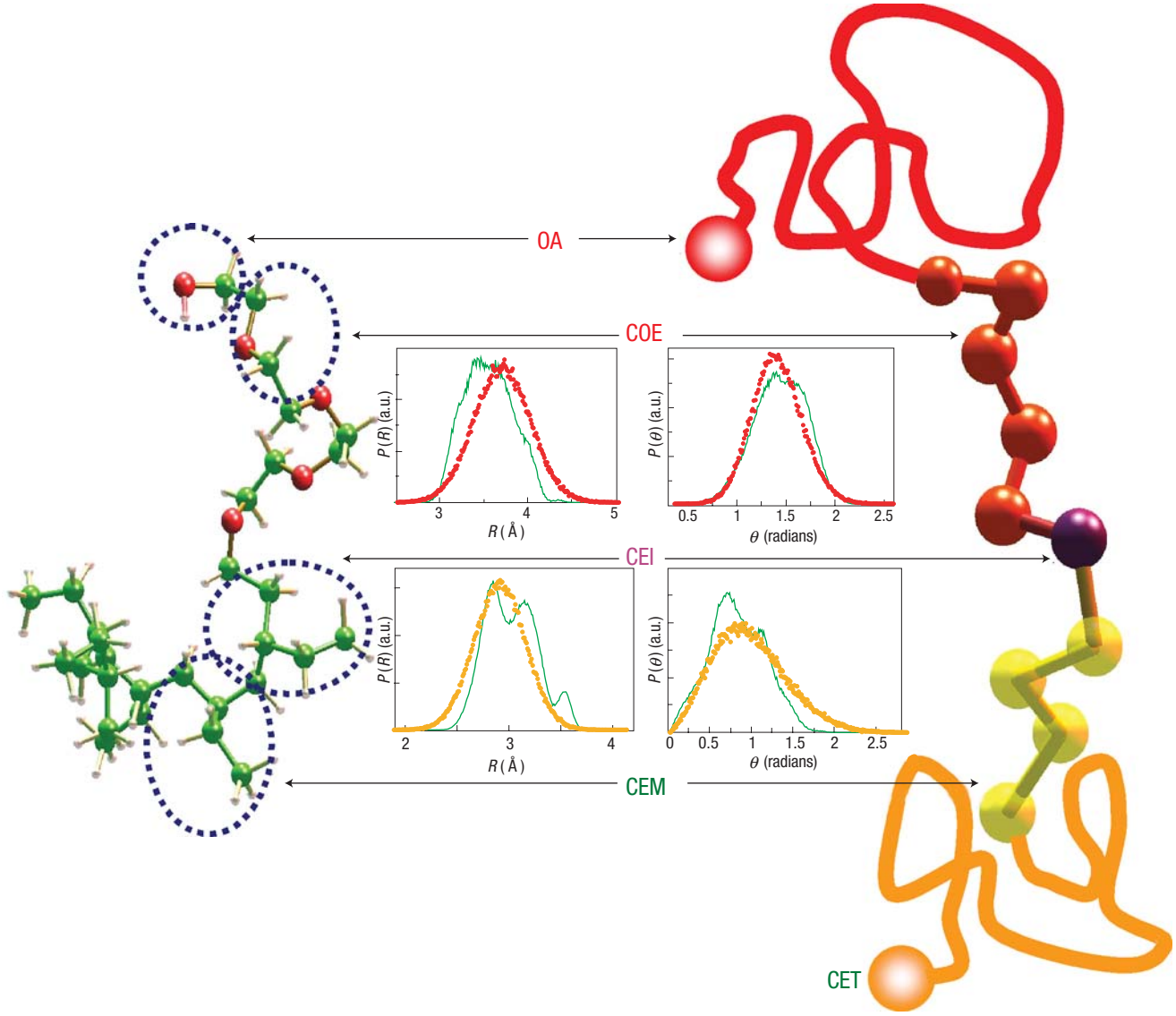

Figure 2 **Coarse-graining scheme used to model a PEO-PEE diblock copolymer**. The all-atom representation is shown on the left hand part of the CG structure is shown on the right. Monomer units EO and EE are represented by COE and CEM, while CEI represents the interfacial unit. End groups, namely tertiary butyl and CH_2-OH are represented by CET and OA, respectively. Colour code for the all-atom representation: oxygen, red; carbon, green; and hydrogen, white; CG model colour code is similar to that of Fig. 1. The inset shows the comparison of bond distance and bond angle distributions for COE (top) and CEM (bottom) units obtained from all-atom (line) and CG (symbols) simulations, respectively. a.u. arbitrary units.

polymers yield an exponent $\varsigma \approx 0.5$, consistent with the experimental results. In contrast, for the lower MW systems ($d < 7$ nm), simulation shows $\varsigma \approx 0.82$. The latter scaling suggests strong stretching even beyond the strong segregation limit for flexible chains. This finding is consistent with the appearance of a 'methyl trough' in the profiles of the smaller MW polymers. Indeed, the density profile of the smallest copolymer (that is, $EO_{10}EE_9$; where EO is ethylene oxide and EE is ethylene-ethylene) is strikingly similar to that of a common phospholipid (dimyristoyl phosphatidylcholine) (Fig. 3a). As the membrane becomes thicker, the density dip at the mid-plane that is typical of lipid bilayers becomes dramatically smoothed. The merging or 'melting' of the two leaflets of the bilayer presumably results from an effective increase in chain flexibility that opposes strong segregation and stretching due to interfacial tension. The classical strong segregation limit exponent of 2/3 is thus reduced to an exponent of 1/2 that is more typical of three-dimensional melts. This insight proves useful to understanding distinctions with lipid as well as the novel properties of high-MW copolymer membranes.

As tension is applied to any membrane, the area per molecule increases, while it is being resisted by interfacial exposure. This increase in area with tension is shown in Fig. 4 for all six simulated systems. In each case, calculated values of area per polymer (A) corresponding to $\tau = 0$ are reported in Table 1. The area elastic modulus (k_a) is related to dilation ($\alpha = \Delta A/A_0$, ΔA being the variation in area) by:

$$\tau = k_a (\Delta A/A_0) \qquad (2)$$

where A_0 is identified at $\tau = 0$. In Fig. 4, the solid line shows the average behaviour of all the systems. k_a is obtained from the average fit. Hence, we conclude that the elastic modulus is nearly invariant over the

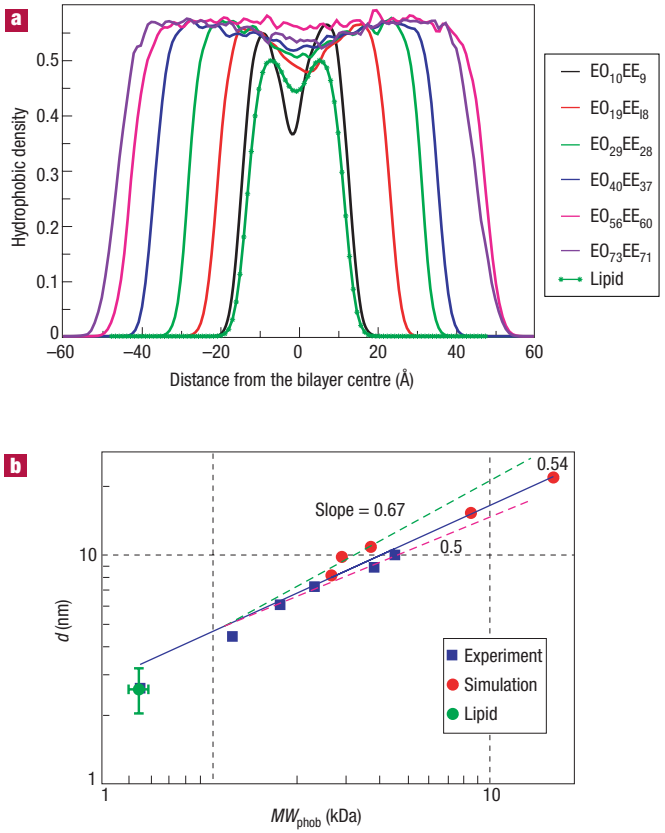

Figure 3 **Membrane core dimensions versus MW_{phob}. a**, Density profiles of hydrophobic blocks for six different systems with constant f_{phil} and variable MW. From inside–out the profiles are in increasing order of MW. The thickness of each system is determined by calculating the peak-to-peak distance at the half-height of the density profile. For comparison, a biological lipid tail density is also shown in the same figure. **b**, Scaling of hydrophobic thickness with MW_{phob}. Symbols show experimental and simulation results and the full line is the linear fit. A natural lipid bilayer thickness is also shown for comparison. Best fit to simulation results yields an exponent value ~0.5.

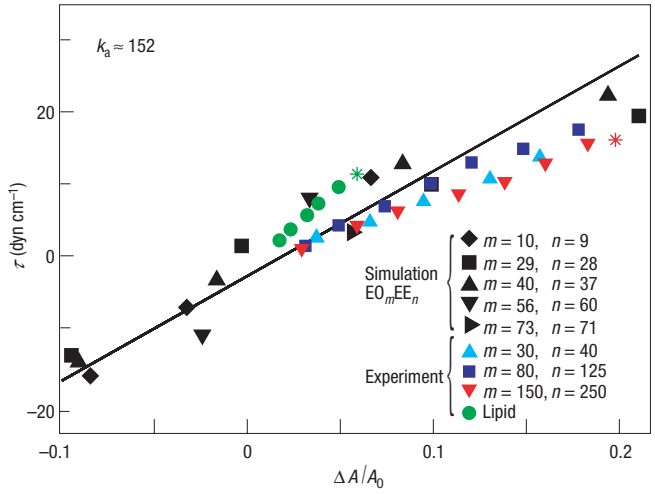

Figure 4 **Master plot of membrane tension versus dilation curves for a wide range of diblock copolymer systems.** All the six systems studied by CG-MD simulation show nearly the same dilational behaviour as shown by the solid line. The slope of this line, k_a, proves to be very close to measurements made on giant vesicles in experiment. Experimental results for a biological lipid are also shown. The point of membrane lysis is observed in experiments for liposomes and select polymersomes as shown here, respectively, by green and red stars.

simulated thickness range of 2–13 nm. As noted by Goetz and Lipowsky[27,42], in the case of uncoupled monolayers, free to slide past one another, the area elastic modulus (k_a) is related to the bending rigidity (k_c) by the following equation:

$$k_c = k_a d^2 \beta \quad (3)$$

Where β = 1/48. For the completely coupled monolayers β = 1/12. Membrane bending analyses in these copolymer simulation systems are not possible as the total area is too small to even perform a normal mode analysis of thermal undulations[27]. CG lipid simulations[27] as well as recent experiments[44] on polymersomes show scaling as per equation (3). This implies that continuum properties such as τ, γ, k_a apply to these nanoscale amphiphilic systems.

Experiment also shows that k_a is constant within about 10% over a fivefold range in MW. A simple area-elasticity calculation[18,45] based on balancing molecular compression against interfacial energy gives $k_a = 4\gamma$. Simulations here imply $\gamma \approx 38$ pN nm^{-1}. For reference, a purely hydrophobic water interface has $\gamma \sim 52$ pN nm^{-1} (ref. 46). The reduction may be due to the hydrophilic (polyEO or PEO) segments at the interface. Indeed, the interfacial tension has long been theorized to reflect the chemistry just at or near the interface and to obey the relation $\gamma \approx \sqrt{\chi}$, where χ is the relevant Flory interaction parameter. Changing the block-copolymer chemistry (for example, polystyrene or polylactic acid[5,9] hydrophobic blocks) is therefore most likely to influence γ through χ. Elasticity determinations through simulation as well as experiment should thus prove particularly revealing of the interactions that drive segregation and generate the interfaces. Likewise, the present simulation results make it relatively clear that lateral interactions between EO groups do not contribute to γ, because such interactions—hydrogen bonds, for example—would almost certainly tend to scale with chain length.

With increased stretching of the membranes the smallest lipid-sized copolymer proves unable to sustain high strains. The higher-MW copolymer membranes could, in contrast, withstand strains approaching 20% or more. Despite potential complications of strain rate for rupture, the CG-MD simulation findings (Fig. 4) are consistent with experimental observations that show lipid membranes rupture at strains of ~5% (green star) or less, whereas the much thicker copolymer membranes rupture at ~20% strains (red star) or higher (off-scale).

In Fig. 5, separated density profiles for the two leaflets of the membrane cores are plotted for the various polymer membranes. As shown in the left panel, the overlap thickness clearly increases with increasing chain length. This tends to smear out the summed density profiles as shown in Fig. 3a. The likely basis for this increased interdigitation of chains is shown in the right panel where density distributions for just the chain ends of PEE are plotted for each leaflet. With increasing chain length, the chain ends increasingly span across the hydrophobic core region. As this interdigitation increases with chain length, chains extend and increasingly entangle.

A quantitative comparison of the relative extent of chain overlap with experimental measurements of diffusivity is shown in Fig. 6 as a function MW_{phob}. As can be seen, the overlap increases rapidly for the smaller chains compared with that of longer chains. This is consistent with the density profile of Fig. 3 that suggests low-MW copolymers are relatively stiff but high-MW copolymers are flexible. Clearly, two

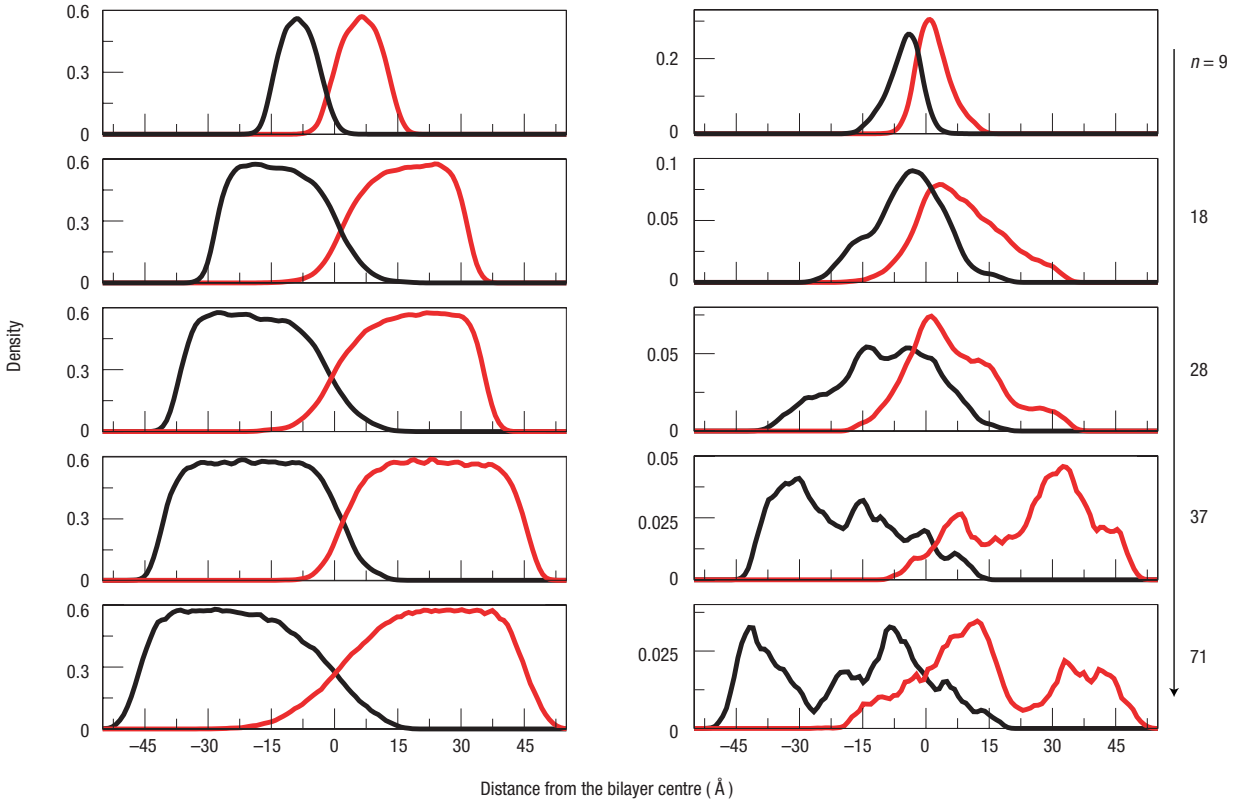

Figure 5 **Density profiles revealing the chain entanglement and interdigitation.** Density profiles of hydrophobic segments of the various polymersomes studied via CG-MD simulation. The number of hydrophobic segments (*n*) in the corresponding copolymer is indicated in the figure. **Left panel:** Density profiles of hydrophobic blocks in each leaflet of the corresponding bilayer are drawn in red and black, respectively. **Right panel:** Density profiles of the hydrophobic tail ends alone are shown. The left panel shows that the extent of overlap or interdigitation of hydrophobic segments increases with chain length and/or MW; the right panel demonstrates that the chain entanglement increases in the same direction.

distinct regimes exist with an abrupt crossover at a $MW_{phob} \approx 1.7$ kDa. This provides an explanation for the experimental measurements of copolymer diffusion in polymer vesicle membranes. The experiments likewise show a crossover from simple Rouse-like lateral mobility to a more complicated activated reptation for hydrophobic molecular weights > 2 kDa (refs 47,48).

To generate further insight into the entanglement mechanism, configurations of individual copolymer chains in the simulation were examined. A typical snapshot of two entangled copolymers is shown in Fig. 6b. Such entanglements are not observed with the smaller-MW block copolymers where the chains appear short, stiff and straight. The difference suggests that the observed trends in diffusional dynamics

Table 1 Description of various copolymers studied in this work. The number of water sites (N_{water}) needed to hydrate a specific number of copolymers (N_{poly}) increases with increasing chain length. The hydrophilic fraction in each chain is represented by f_{phil}. The molecular weight of each chain is denoted by MW while the respective hydrophobic mass is represented by MW_{phob}. The hydrophobic core thickness (*d*) and area per polymer chain (*A*) are listed only for pre-assembled bilayer structures. For the worm and spherical structures *d* denotes the diameter.

Copolymer	N_{poly}/N_{water}	f_{phil} (%)	MW/MW_{phob} (kDa)	*A* (Å²)	Morphology	*d* (nm)
$EO_{10}EE_{9}$	108/2,160	45.6%	1.03/0.50	67.07	Bilayer	2.63
$EO_{19}EE_{18}$	128/4,000	44.8%	1.93/1.00	76.10	Bilayer	4.38
$EO_{29}EE_{28}$	128/4,265	44.5%	2.93/1.57	94.34	Bilayer	5.99
$EO_{40}EE_{37}$	128/7,776	45.6%	3.92/2.07	104.2	Bilayer	7.68
$EO_{57}EE_{60}$	96/8,520	42.6%	5.96/3.36	134.3	Bilayer	8.66
$EO_{73}EE_{71}$	96/10,368	44.5%	7.28/3.98	146.4	Bilayer	9.79
$EO_{21}EE_{37}$	100/7,000	30.9%	3.08/2.07	-	Bilayer	8.55
$EO_{50}EE_{37}$	64/7,680	51.1%	4.36/2.07	-	Worm	6.01
$EO_{92}EE_{37}$	48/24,000	65.6%	6.21/2.07	-	Spherical	4.83

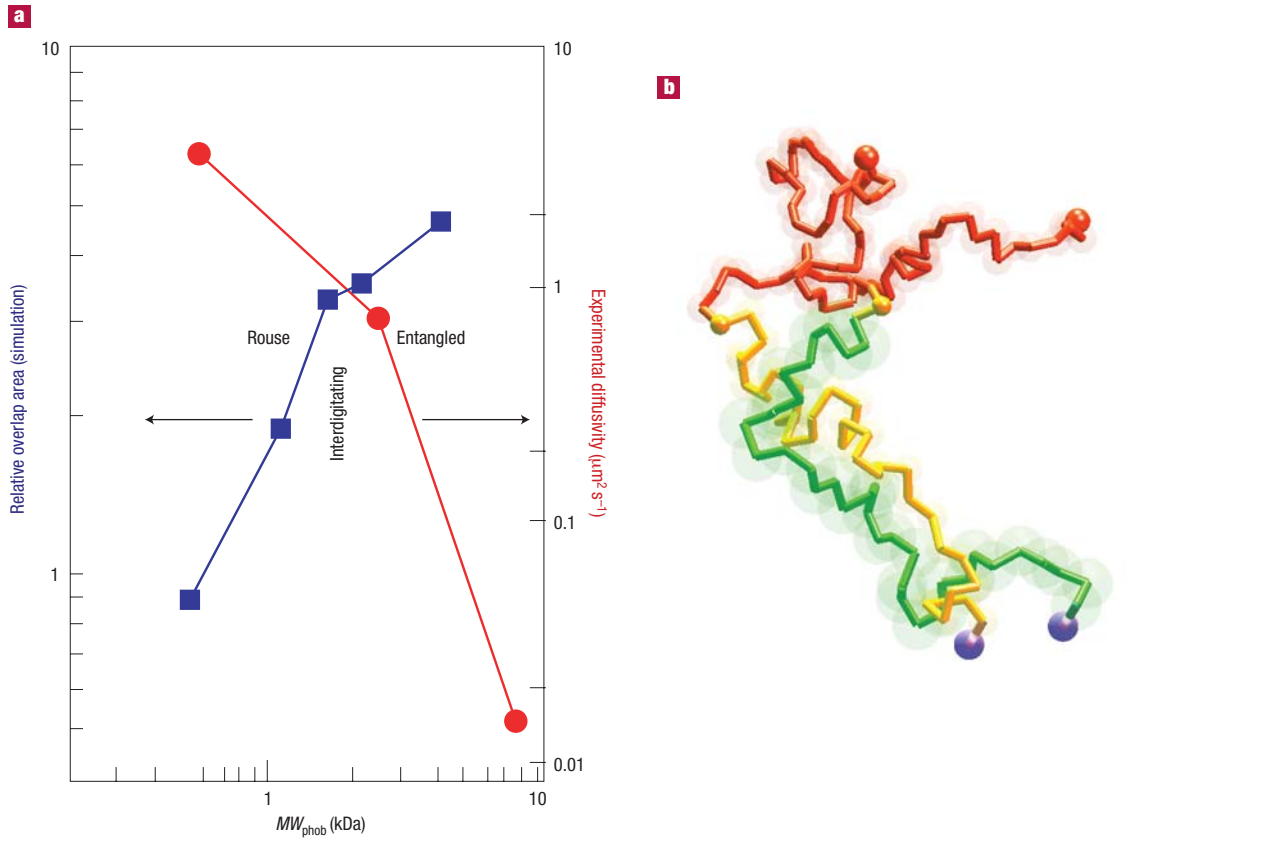

Figure 6 **Chain overlap, experimental diffusivity, and chain entanglements. a**, The extent of hydrophobic tail overlap observed in simulations is plotted with lateral diffusion measurements made as a function of MW_{phob}; the diffusion constants at room temperature were corrected to have the same monomer friction factor. The region of Rouse-like lateral mobility is also indicated. **b**, Simulation snapshot of two entangled EO_mEE_n block copolymer chains. For clarity, the hydrophobic (EE) blocks of two chains are shown in two different colours (yellow and green).

originate in configurational arrangements such as entanglements that are fostered by increasingly interdigitated and flexible chains.

In conclusion, by carrying out CG-MD simulations on diblock copolymers in water we showed that the copolymer hydrophilic fraction f_{phil} plays a crucial role in determining the final morphology of the self-assembling system as known experimentally. In addition to providing molecular-level insight for such observations, the present CG simulation study also complements the experiments. For example, the MW dependence of the hydrophobic thickness reveals that only large MW polymers follow the $\zeta \approx 0.5$ trend seen experimentally. Smaller MW systems (with $d < 7$ nm) were not explored in experimental studies but yielded $\zeta \approx 0.82$ in simulation, which indicates more stretched and ordered configurations consistent with lipids. The area elastic-modulus values obtained from the CG simulations are in qualitative agreement with the experimental results. Additionally, k_a is found to be nearly invariant with hydrophobic thickness and MW. This is in accordance with recent experiments, which concluded that the elastic modulus is solely determined by the chemical composition of the interfacial units[18].

The computed density profiles provide distinctive insight into polymersome structure. It is observed that unlike lipid bilayers that show a definitive density depletion (methyl trough) in their interior, monodisperse block copolymers show only a minimal density dip with increasing MW. Neutron scattering and other methods should be able to probe such trends given a set of suitably modified copolymers. However, it is already clear from profiles of individual leaflets of the bilayers that with increasing copolymer MW, the core chain-ends bend and localize increasingly at the aqueous interface. Chain entanglement thereby combines with chain overlap (interdigitation) to decrease the lateral mobility of the diblocks in thicker membranes. Overall, the CG simulation results compare well with the many experimental observations on a series of PEO–polybutadiene and PEO–PEE diblocks, suggestive of the generic nature of the current model. This suggests that although the current CG model is developed based on this chemistry, the methods can be readily extended to study the structure and properties of other block copolymers such as PEO–polylactic acid and others[5]. The CG approach herein would thus seem to offer a rational design tool for synthesis of novel, block-copolymer architectures.

METHODS

The detailed description of CG parameterization[28,38] is described in the Supplementary Information, but the necessary details are mentioned briefly in the following. To study the self-assembly, the simulation system is constructed by initially distributing CG polymer chains on a three-dimensional cubic lattice and hydrating the resulting system with sufficient CG water W sites. The resulting simulation system contains EO/EE copolymers and water with the ratio shown in Table 1. This system is then equilibrated at the desired thermodynamic state (298.15 K temperature and 1 atm. pressure) by keeping the polymers immobile. This results in a suitable initial unbiased lattice configuration. Because we aim to study natural self-assembly, in order to avoid unwanted compressions/expansions during the simulations, an isobaric NPT ensemble is used. This ensemble isotropically compresses/expands the box lengths, in contrast to general NPT ensemble.

On the other hand, for the pre-assembled cases, the simulation system is constructed in a box by replicating a basic unit containing four polymer chains (two in the upper leaflet and two in the lower leaflet) with sufficient CG water W sites. Polymer chains are placed in such a way that the hydrophobic tails face each other, while the hydrophilic parts are exposed to water. This system is allowed to relax and equilibrate at 298.15 K. We then replicated the simulation cell in the *xy* plane to generate polymer systems with, respectively 8, 16, 32, 64 and 128 polymers. After delicate adjustments to remove overlapping waters, the simulation systems resulted in the copolymer/water ratios presented in Table 1.

In order to compare our simulation results with the experimental results, it is necessary to carry out MD simulations with constant surface area per polymer (A) that corresponds to zero tension. This is an important observation because the surface/interfacial tension of the system is very sensitive to the quantity A and can vary over an order of magnitude by moderately changing surface area. Hence, for this purpose we have chosen an N_APT ensemble. In this ensemble, the simulation box length in the x and y directions is fixed while it is allowed to vary in the z direction. As a result, the normal pressure in the z direction fluctuates around a mean (pressure) value, while keeping the surface area per polymer unchanged. More details in this regard are presented in the Supplementary Information.

The simulation system in each case was allowed to relax and equilibrate at 298.15 K for 5 ns. For the next 5 ns, the stability of the system was monitored. As mentioned in earlier studies, the CG approach involves larger size interacting sites and softer potentials, which essentially results in the timescales that are dilated by two orders of magnitude larger in comparison with the all-atom simulation times. All of the times reported in this article are the actual CG simulation times, and not the effective simulation times, which are probably two orders of magnitude longer.

Received 17 February 2004; accepted 17 June 2004; published 8 August 2004.

References

1. Discher, B. M. *et al.* Polymersomes: Tough vesicles made from diblock copolymers. *Science* 284, 1143–1146 (1999).
2. Cornelissen, J. L. M., Fisher, M., Sommerdijk, N. A. J. M. & Nolte R. J. M. Helical superstructures from charged poly(styrene)-poly(isocyanodipeptide) block copolymers. *Science* 280, 1427–1430 (1998).
3. Meier, W., Nardin, C. & Winterhalter, M. Reconstitution of channel proteins in (polymerized) ABA triblock copolymer membranes. *Angew. Chem. Int. Edn* 39, 4599–4602 (2000).
4. Nardin, C., Widmer, J., Winterhalter, M. & Meier, W. Amphiphilic block copolymer nanocontainers as bioreactors. *Eur. Phys. J. E* 4, 403–410 (2001).
5. Okada, J., Cohen, S. & Langer, R. In-vitro evaluation of polymerized liposomesas an oral-drug delivery system. *Pharmaceut. Res.* 12, 576–582 (1995).
6. Discher, D. E. & Eisenberg, A. Polymer vesicles. *Science* 297, 967–973 (2002).
7. Hamley, I. W. Nanostructure fabrication using block copolymers. *Nanotechnology* 14, R39–R54 (2003).
8. Napoli, A. V., Valentini, M., Tirelli, N., Müller, M. & Hubbell, J. A. Oxidation-responsive polymeric vesicles. *Nature Mater.* 3, 183–189 (2004).
9. Zhang, L. F. & Eisenberg, A. Multiple morphologies of crew-cut aggregates of polystyrene-B-poly(acrylic acid) block-copolymers. *Science* 268, 1728–1731 (1995).
10. Jain, S. & Bates, F. S. On the origins of morphological complexity in block copolymer surfactants. *Science* 300, 460–464 (2003).
11. Tew, G. N. *et al.* De novo design of biomimetic antimicrobial polymers. *Proc. Natl Acad. Sci. USA* 99, 5110–5114 (2002).
12. Lipowsky R, & Sackman, E. (eds) *Structure and Dynamics of Membranes* (Elsevier, Amsterdem, 1995).
13. Cevc, G. *Phospholipids Handbook* (Marcel Decker, New York, 1993).
14. Chakraborty, A. K. & Golumbfskie, A. J. Polymer adsorption driven self-assembly of nanostructures. *Ann. Rev. Phys. Chem.* 52, 537–573 (2001).
15. Balsara, N. P., Garetz, B. A., Newstein, M. C., Bauer, B. J. & Prosa, T. J. Evolution of microstructure in the liquid and crystal directions in a quenched block copolymer melt. *Macromolecules* 31, 7668–7675 (1998).
16. Forster, S., Zisenis, M., Wenz, E. & Antonietti, M. Micellization of strongly segregated block copolymers. *J. Chem. Phys.* 104, 9956–9970 (1996).
17. Needham, D. & Zhelev, D. V. *The Mechanochemistry of Lipid Vesicles Examined by Micropipette Manipulation Techniques in Vesicles* (ed. Rosoff, M.) Ch. 9 (Marcel Dekker, New York, 2000).
18. Bermudez, H., Brannan, A. K., Hammer, D. A., Bates, F. S. & Discher, D. E. Molecular weight dependence of polymersome membrane structure, elasticity, and stability. *Macromolecules* 35, 8203–8208 (2002).
19. Hillmyer, M. A. & Bates, F. S. Synthesis and characterization of model polyalkane-poly(ethylene oxide) block copolymers. *Macromolecules* 29, 6994–7002 (1996).
20. Pakula, T., Karatasos, K., Anastasiadis, S. H. & Fytas, G. Computer simulation of static and dynamic behavior of diblock copolymer melts. *Macromolecules* 30, 8463–8472 (1997).
21. Schultz, A. J., Hall, C. K. & Genzer, J. Computer simulation of copolymer phase behavior. *J. Chem. Phys.* 117, 10329–10338 (2002).
22. Pastor, R. W., Venable, R. M., Karplus, M. & Szabo, A. A simulation based model of nmr T1 relaxation in lipid bilayer vesicles. *J. Chem. Phys.* 89, 1128–1140 (1988).
23. Noguchi, H. & Takasu, M. Fusion pathways of vesicles: A Brownian dynamics simulation. *J. Chem. Phys.* 115, 9547–9551 (2001).
24. Noguchi, H. Fusion and toroidal formation of vesicles by mechanical forces: A Brownian dynamics simulation. *J. Chem. Phys.* 117, 8130–8137 (2002).
25. Srinivas, G. & Bagchi, B. Detection of collapsed and ordered polymer structures by fluorescence resonance energy transfer in stiff homopolymers: Bimodality in the reaction efficiency distribution. *J. Chem. Phys.* 116, 837–844 (2002).
26. Smit, B. *et al.* Structure of a water/oil interface in the presence of micelles: a computer simulation study. *J. Phys. Chem.* 95, 6361–6368 (1991).
27. Goetz, R., Gompper, G. & Lipowsky, R. Mobility and elasticity of self-assembled membranes. *Phys. Rev. Lett.* 82, 221–224 (1999).
28. Shelley, J. C., Shelley, M. Y., Reeder, R. C., Bandyopadhyay, S. & Klein, M. L. A coarse grain model for phospholipid simulations. *J. Phys. Chem. B* 105, 4464–4470 (2001).
29. Tieleman, D. P. & Marrink, S. J. Potential of mean force of a lipid in a lipid bilayer. *Biophys. J.* 84, 368–369 (2003).
30. Tieleman, D. P., Leontiadou, H., Mark, A. E. & Marrink, S. J. Simulation of pore formation in lipid bilayers by mechanical stress and electric fields. *J. Am. Chem. Soc.* 125, 6382–6383 (2003).
31. Marrink, S. J. & Tieleman, D. P. Molecular dynamics simulation of a lipid diamond cubic phase. *J. Am. Chem. Soc.* 123, 12383–12391 (2001).
32. Marrink, S. J., Lindahl, E., Edholm, O. & Mark, A. E. Simulation of the spontaneous aggregation of phospholipids into bilayers. *J. Am. Chem. Soc.* 123, 8638–8639 (2001).
33. Marrink, S. J. & Mark, A. E. Effect of undulations on surface tension in simulated bilayers. *J. Phys. Chem. B* 105, 6122–6127 (2001).
34. Marrink, S. J. & Mark, A. E. Molecular dynamics simulation of the formation, structure, and dynamics of small phospholipid vesicles. *J. Am. Chem. Soc.* 125, 15233–15242 (2003).
35. Nielsen, S. O. & Klein, M. L. *Bridging Time Scales: Molecular Simulations for the Next Decade* (eds Nielaba, P., Mareschali, M. and Ciccotti, G.) 27–63 (Elsevier Science, Amsterdam, 2003).
36. Shelley, J. C. *et al.* Simulations of phospholipids using a coarse grain model. *J. Phys. Chem. B* 105, 9785–9792 (2001).
37. Nielsen, S. O., Lopez, C. F., Moore, P. B., Shelley, J. C. & Klein, M. L. Molecular dynamics investigations of lipid langmuir monolayers using a coarse-grain model. *J. Phys. Chem. B* 107, 13911–13917 (2003).
38. Srinivas, G., Shelley, J. C., Nielsen, S. O., Discher, D. E. & Klein, M. L. Simulation of diblock copolymer self-assembly using a coarse-grain model. *J. Phys. Chem. B* 108, 8153–8160 (2004).
39. Lindahl, E. & Edholm, O. Spatial and energetic-entropic decomposition of surface tension in lipid bilayers from molecular dynamics simulations. *J. Chem. Phys.* 113, 3882–3893 (2000).
40. Feller, S. E., Zhang, Y. H. & Pastor, R. W. Computer-simulation of liquid/liquid interfaces. 2. Surface-tension area dependence of a bilayer and monolayer. *J. Chem. Phys.* 103, 10267–10276 (1995).
41. Feller, S. E. & Pastor, R. W. Constant surface tension simulations of lipid bilayers: The sensitivity of surface areas and compressibilities. *J. Chem. Phys.* 111, 1281–1287 (1999).
42. Goetz, R. & Lipowsky, R. Computer simulations of bilayer membranes: self-assembly and interfacial tension. *J. Chem. Phys.* 108, 7397–7409 (1998).
43. Rao, M. & Levesque, D. Surface structure of a liquid film. *J. Chem. Phys.* 65, 3233–3236 (1976).
44. Bermudez, H., Hammer, D. A. & Discher, D. E. Effect of bilayer thickness on membrane bending rigidity. *Langmuir* 20, 540–543 (2004).
45. Israelachvili, J. N. *Intermolecular and Surface Forces* (Academic, San Diego, California, 1998).
46. Mark, J. E. *Physical Properties of Polymers Handbook* (AIP Series in Polymers and Complex Materials, AIP, New York, 1996).
47. Lee, J. C. M., Law, R. J. & Discher, D. E. Bending contributions hydration of phospholipid and block copolymer membranes: Unifying correlations between probe fluorescence and vesicle thermoelasticity. *Langmuir* 17, 3592–3597 (2001).
48. Lee, J. C. M., Santore, M., Bates, F. S. & Discher, D. E. From membranes to melts, rouse to reptation: Diffusion in polymersome versus lipid bilayers. *Macromolecules* 35, 323–326 (2002).

Acknowledgements

We would like to thank John C. Shelley, Carlos Lopez, Steve Nielsen, Ivaylo Ivanov and Preston B. Moore. This work has been supported by the National Science Foundation (Pennsylvania University's Materials Research Science and Engineering Centre) and the National Institutes of Health.

Correspondence and requests for materials should be addressed to M.L.K.

Supplementary Information accompanies the paper on www.nature.com/naturematerials

Competing financial interests

The authors declare that they have no competing financial interests.